Synthesis and Characterization of Rutile TiO$_2$ Nanoparticles for the Toxicological Effect on the H9c2 Cell Line from Rats

Pamela Santos-Aguilar, Judith Bernal-Ramírez, Eduardo Vázquez-Garza, Lydia Yerid Vélez-Escamilla, Omar Lozano, Gerardo de Jesús García-Rivas,* and Flavio F. Contreras-Torres*

Read Online

ACCESS | Metrics & More | Article Recommendations

ABSTRACT: The widespread use of titanium dioxide (TiO$_2$) has raised concerns about potential health risks associated with its cytotoxicity in the cardiovascular system. To evaluate the cytotoxicity of TiO$_2$ particles, the H9c2 rat cardiomyoblasts were used as a biological model, and their toxicological susceptibility to TiO$_2$-anatase and TiO$_2$-rutile particles was studied in vitro. The study examined dose and time exposure responses. The cell viability was evaluated based on metabolic inhibition and membrane integrity loss. The results revealed that both TiO$_2$-anatase and TiO$_2$-rutile particles induced similar levels of cytotoxicity at the inhibition concentrations IC$_{25}$ (1.4−4.4 μg/cm^2) and IC$_{50}$ (7.2−9.3 μg/cm^2). However, at more significant concentrations, TiO$_2$-rutile appeared to be more cytotoxic than TiO$_2$-anatase at 24 h. The study found that the TiO$_2$ particles induced apoptosis events, but necrosis was not observed at any of the concentrations of particles used. The study considered the effects of microstructural properties, crystalline phase, and particle size in determining the capability of TiO$_2$ particles to induce cytotoxicity in H9c2 cardiomyoblasts. The microstress in TiO$_2$ particles was assessed using powder X-ray diffraction through Williamson−Hall and Warren−Averbach analysis. The analysis estimated the apparent crystallite domain and microstrain of TiO$_2$-anatase to be 29 nm ($\varepsilon = 1.03\%$) and TiO$_2$-rutile to be 21 nm ($\varepsilon = 0.53\%$), respectively. Raman spectroscopy, N$_2$ adsorption isotherms, and dynamic light scattering were used to identify the presence of pure crystalline phases (>99.9%), comparative surface areas (10 m^2/g), and ζ-potential values (−24 mV). The difference in the properties of TiO$_2$ particles made it difficult to attribute the cytotoxicity solely to one variable.
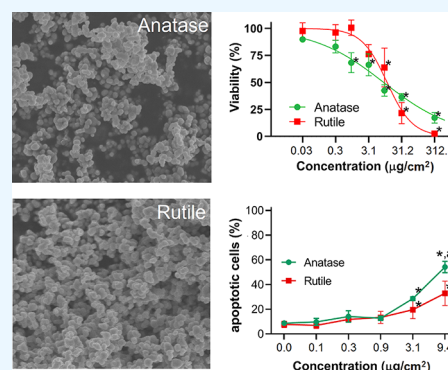
1. INTRODUCTION

Titania (TiO$_2$, titanium dioxide), an inorganic material with high chemical stability and versatile properties, finds extensive applications in a variety of commercial products. Its anticorrosive, photocatalytic, and optoelectronic properties make it an attractive material for use in various fields, including plastics, paints, varnishes, papers, inks, personal skin care products, cosmetics, sunscreens, toothpaste, photovoltaic cells, wastewater treatments, and bactericidal agents.[1] Additionally, TiO$_2$ has garnered interest in biomedical applications, including photodynamic cancer therapy, drug delivery systems, cell imaging, biosensors for biological assay, and genetic engineering.[2] Moreover, the Food and Drug Administration (FDA) has permitted the use of TiO$_2$ as an additive in food and pharmaceutical products.[3,4] Despite the broad field of applications, the extensive production and use of TiO$_2$ products worldwide[5,6] warrant consideration of their potential effect in human health.[7] The association and internalization of TiO$_2$ particles in cells, migration and accumulation in organs, and mechanisms of inhalation, ingestion, or skin absorption all provide perspectives on the impact of using TiO$_2$ in living

organisms.[8−17] Therefore, the potential risks associated with the use of different titania-based products deserve attention.

One area of concern in the use of TiO$_2$ is its presence in food and personal care products.[18] Food-grade TiO$_2$ particles, such as E171 with a size of 112 nm, have been associated with alterations in gut microbiota composition and multiple pathways in the liver and colon of obese mice when consumed in a Western diet.[19] Exposure to TiO$_2$ particles through inhalation,[1,5] absorption through slightly damaged skin,[14,15,20] and oral administration[10,11] can also pose a risk to several systemic organs.[11−13,16,17,21] Therefore, toxicological studies have been conducted using different biological models[20−33] to assess dose−response data. In the cardiovascular system, which is our area of interest, the first in vitro evaluation using H9c2 cardiomyoblasts reported severe cell damage by decreasing the

mitochondrial membrane potential due to the accumulation of particles in the cytoplasm.[24] In a recent study by Colin-Val and colleagues,[21] the toxicity of food-grade TiO$_2$ particles with sizes ranging from 130 to 330 nm was evaluated in H9c2 cells and ex vivo rat hearts. The study suggested that consuming TiO$_2$ particles as a food additive may lead to the development of cardiovascular disease. Additionally, in vivo assays[17] in mice have demonstrated myocardial damage, oxidative stress, inflammation, and atherosclerosis effects when animals were exposed to TiO$_2$ particles. However, it is worth noting that none of these studies[17,21,24] examined the differential cytotoxicity comparatively with pure TiO$_2$-anatase and TiO$_2$-rutile particles. Consistently with the literature survey findings,[10–13,16,17,21,24,30] the type of cell death observed in vitro and the mechanisms of the inflammatory response observed in vivo caused by TiO$_2$ particles are yet to be fully established in myocardial cells.

The H9c2 cell line might represent a suitable model that can accurately mimic the hypertrophic responses of primary cardiac myocytes.[34] In this study, we measured the metabolic activity, membrane integrity, intracellular redox state, and mitochondrial superoxide production in H9c2 cardiomyoblasts to investigate the impact of TiO$_2$ particles in connection with their physicochemical characteristics.[26–29,31,35,36] The present study aims to evaluate the cytotoxicity of TiO$_2$ particles comparatively (i.e., anatase and rutile) and differentially (i.e., materials properties) in H9c2 rat cardiomyoblasts. To our knowledge, this is the first study to comprehensively evaluate the cytotoxicity of TiO$_2$-rutile particles in the H9c2 cell line. Notably, previous studies[21,24] conducted on H9c2 cells used food-grade anatase. Our study expands upon this previous research by evaluating the cytotoxicity of pure TiO$_2$-anatase and TiO$_2$-rutile, providing a more comprehensive understanding of the potential health effects of these particles on cardiac cells. This distinction between TiO$_2$-anatase and TiO$_2$-rutile may also be relevant in cardiomyocytes and could potentially have implications for human health. To achieve the main objective, we prepared and characterized TiO$_2$-anatase and TiO$_2$-rutile particles and evaluated their cytotoxicity in H9c2 cells. Our findings suggest that microstructure, crystalline phase, and particle size of TiO$_2$ particles significantly contributed to cytotoxicity in H9c2 cells. Notably, we observed that the extent of cytotoxicity varied depending on whether the particles were TiO$_2$-anatase or TiO$_2$-rutile, and this differentiation was dose-dependent.

2. MATERIALS AND METHODS

2.1. Materials and TiO$_2$ Preparation. The two polycrystalline titania samples used in this study were prepared from titanium IV oxide powder (5% rutile, 325 mesh). To obtain the pure TiO$_2$-anatase phase, the raw powder (Sigma-Aldrich, 248576) was calcined in an electric muffle furnace set at 400 °C for 24 h with a heating rate of 20 °C/min. The phase transformation from anatase to rutile was carried out following a well-established heat treatment method.[23,37] Specifically, the TiO$_2$-anatase phase was calcined in an electric muffle furnace set at 1000 °C for 24 h with a heating rate of 20 °C/min to obtain the pure TiO$_2$-rutile phase.

2.2. Particle Characterization. Scanning electron microscopy (SEM) was carried out using a Nova NanoSEM 200 (FEI, Hillsboro, OR) field emission−scanning electron microscope functioning at 15 kV. The micrographs with at least a magnification of 50,000× were analyzed using ImageJ software

to estimate each particle's respective areas (averaged for >200 particles per sample). The hydrodynamic size was measured using dynamic light scattering (DLS) in a Zeta Sizer Nano S-90 (Malvern; λ_{HeNe} = 632.8 nm; backscattering angle of 173°). Approximately 3 mL suspensions of particles (30, 100, and 200 μg/mL) were dispersed by ultrasonication (160 W, 20 kHz, 5 min) in Milli-Q water. Three replicates of 20 runs of 10 s were performed to obtain the size distribution. The mean hydrodynamic diameter, polydispersity index, and ζ-potential were obtained through the Zetasizer software (DTS v7.11). Raman spectra were acquired on a Cora 5500 Raman spectrometer (Anton Paar, Germany) operating at 784 nm with 300 mW. Raman spectra were accumulated over 600 ms using a spectral resolution of 6 cm^{-1} from 100 to 2300 cm^{-1}. Finally, nitrogen gas adsorption isotherms were measured using a sorptometer Quantachrome Autosorb-1 automated gas sorption analyzer (Quantachrome Instruments, Boynton Beach, FL). Before measurements, samples (approximately 500 mg) were outgassed overnight for 12 h at 200 °C. A typical Brunauer−Emmett−Teller (BET) analysis was conducted to a relative pressure, P/P_0 < 0.3 at 77 K, where P_0 is the saturation pressure.

2.3. Microstructure Characterization. Powder X-ray diffraction (XRD) measurements were performed using Cu Kα radiation (λ_1 = 1.54060 Å, λ_2 = 1.54439 Å; 30 kV, 10 mA) in a Bruker D2-Phaser diffractometer equipped with Bragg ($\theta°−\theta°$) geometry, Ni-Kβ filter, and LyxnEye detector. Diffractograms were recorded from 5° to 120° with a step size of 0.02° (2θ°) for periods of 2 s. The instrumental broadening was estimated by measuring the corundum (Al$_2$O$_3$) standard. The obtained instrumental function[38] parameters were fitted as a function of 2θ°, obtaining the following equation, $H = 8.27 \times 10^{-2} - 8.08 \times 10^{-4} (2\theta°) + 1.08 \times 10^{-5} (2\theta°).$[2]

Phase identification for TiO$_2$-anatase and the TiO$_2$-rutile was determined by comparing the JCPDS Card No. 21-1272 and JCPDS Card No. 21-1276, respectively. Rietveld refinement of the crystalline structures was carried out using the TOPAS suite program. The double-Voigt approach was chosen, and those parameters were used to define the diffraction profile function. Intensity-dependent parameters (atomic parameters) were refined to obtain the atomic positions for Ti and O. The crystal structures were refined in the space groups I_{41}/amd (No. 141) for anatase and P_{42}/mnm (No. 136) for rutile. In the case of TiO$_2$-anatase, the isotropic displacements were refined for Ti-4b (0, 1/4, 3/8) and O-8e (0, 1/4, z). For TiO$_2$-rutile, the isotropic displacements were refined for Ti-2a (0, 0, 0) and O-4f (x, x, 0). The background was the polynomial function of 2θ of the third order. The instrumental profile asymmetry was modeled using asymmetry correction functions with two refinable parameters for 2θ angles lower than 40°. The fittings were satisfactorily obtained by reaching a goodness-of-fit with a chi-square value of less than 3.

The microstructure of TiO$_2$ particles was evaluated according to the Williamson−Hall (WH) and the Warren−Averbach (WA) methods.[39] WH and WA are the most common X-ray line profile analysis that looks for a relationship between the diffraction vector g_{hkl}^2 and the microstrain. The WH method correlates the broadening β as computed by the Scherrer equation adding a new term dependent on crystal imperfection and distortion, ϵ, which is called the apparent lattice strain

$$\beta = \frac{k\,\lambda}{D_{hkl}\cos\theta_B} + 4\epsilon\tan\theta$$

The terms can be rearranged in terms of a new variable, $\tilde{\beta} = \frac{\beta\cos\theta}{\lambda}$, while the interplanar spacing can be defined as $\tilde{d} = \frac{2\sin\theta}{\lambda}$ to obtain the working equation

$$\tilde{\beta} = \frac{1}{\langle\tau\rangle} + 2\epsilon\tilde{d}$$

where the inverse of the intercept $\langle\tau\rangle$ is defined as the apparent crystallite size. From this, the root-mean-square strain can be calculated as $\langle\epsilon_0^2\rangle^{1/2} = \sqrt{\frac{2}{\pi}}\,\epsilon$. The integral breadth of line profiles caused by lattice distortions (strain) is defined as $\beta^D = \sqrt{2\pi^2 g_{hkl}^2\langle\epsilon^2\rangle}$. In this way, the broadening of the diffraction lines can be expressed as the linear contribution of the functions caused by the crystallite size and the microstrain present in the crystalline lattice. The WA method[40] includes the dependence of crystallite size and strain through a Fourier series, $A^s(L)$ and $A^D(L)$, respectively, representing the peak profiles

$$\ln A(g_{hkl}, L) \cong \ln A^s(L) - 2\pi^2 g_{hkl}^2 L^2\langle\epsilon^2\rangle$$

The working variable is the Fourier series defined as $L = na_3$, where $a_3 = \frac{\lambda}{2(\sin\sin\theta_2 - \sin\sin\theta_1)}$. After a linear regression of the coefficients of two reflections at different values of a Fourier variable, the value of $\langle\epsilon^2\rangle$ is determined from the slope's absolute value. The points at $g_{hkl}^2 = 0$ represents the natural logarithm of the size Fourier coefficients, from which the crystallite size can be estimated,

$$A^D(L) = \exp(-2\pi^2 g_{hkl}^2\langle\epsilon^2\rangle L^2)$$

The Fourier coefficients were calculated using a discrete Fourier transform; only the real part of the coefficient was employed for the WA analysis.

2.4. Cell Culture. The H9c2 rat cardiomyoblast cell line (ATCC, CRL-1446) was cultured in Dulbecco's modified Eagle's medium (DMEM) (Sigma-Aldrich, D7777), adding 3.7 g/L sodium bicarbonate (NaHCO$_3$) (Sigma-Aldrich, S6014) filtered through a 0.2 μm Pore CA Membrane (Corning, 430513) and supplemented with 10% heat-inactivated fetal bovine serum, FBS (Biowest), and penicillin−streptomycin solution 1× (Gibco) containing penicillin (100 U/mL) and streptomycin (100 μg/mL). All cultures were incubated at 37 °C in a 5% CO$_2$ and 95% air-humidified atmosphere. The assays were performed in the log growth phase, where the cells replicate exponentially. The medium was replaced every 2−3 days and passaged at 70−80% cell confluence to prevent differentiation or cell fusion. Cell detachment was performed with 0.25% Trypsin−EDTA (Gibco, 25200-072) and cell quantification by Trypan Blue solution (Sigma, T8154) in a Neubauer-improved counting chamber.

2.5. TiO$_2$ Particle Suspensions. A stock of TiO$_2$ particle dispersion (1 mg/mL) in water and DMEM with 10% FBS was prepared based on standard procedures.[41] The stock TiO$_2$ solution was vortexed for 30 s and bath sonicated (Bransonic Ultrasonic Bath, CPXH Series) for 20 min before use and further preparation of dissolutions. The used concentrations for TiO$_2$ particles were traced in μg/cm^2 to follow the FAIR principles[42] in nanotoxicology, and because TiO$_2$ particle

suspensions are unstable and precipitate. In this work, we tested concentrations for 0.03, 0.31, 3.12, 31.25, and 312.5 μg/cm^2 (equivalent to 0.1, 1, 10, 100, and 1000 μg/mL, respectively).

2.6. Viability Assays. H9c2 cells (4 × 10^3 cells/well) in DMEM media were treated with different concentrations of TiO$_2$ particles (0.03, 0.31, 3.12, 31.25, and 312.5 μg/cm^2) for 24 h. After treatment, cells were incubated with 5 mg/mL Alamar Blue (Thermo Fisher) for 2.5 h at 37 °C without light. Fluorescence (excitation at 530 nm and emission at 590 nm) was measured using a microplate BioTek Synergy HT. The normalized response described by Hill−Langmuir equation was fitted to

$$f(x) = \frac{100}{1 + \left(\frac{IC_{50}}{x}\right)^H}$$

through a nonlinear regression, and thus the half-maximal inhibitory concentration (IC$_{50}$) was obtained for each treatment analyzing the inhibitor concentration versus the normalized response. Subsequently, the inhibitor concentration for other percentages different than 50% was calculated as follows

$$x = IC_{50}\left(\frac{100 - y}{y}\right)^{1/H}$$

where y can take 25% (IC$_{25}$) and 75% (IC$_{75}$) and x is the looked-for inhibitor concentration. The viability percentage was computed as follows

$$\text{viability}\,(\%) = \frac{\text{sample} - \text{blank}}{\text{control} - \text{blank}} \times 100$$

sample, control, and blank represent the average fluorescence values for each particle treatment, no-treatment, and no-cell well, respectively.

2.7. Cell Death. H9c2 cells were exposed to several TiO$_2$ treatments (0.1, 0.3, 0.9, 3.1, and 9.4 μg/cm^2) for 24 h (dose-dependent) and exposed to 0.9 μg/cm^2 TiO$_2$ particles for 12, 24, and 48 h (time-dependent). Thus, cells were incubated with 5 μL of Annexin V-FITC (E_x = 488 nm; E_m = 530 nm) or 5 μL of 7-AAD (E_x = 488 nm; E_m = 647 nm) in FACS tubes, which were incubated for 15 min at RT in the darkness. Then, the cells were washed once by centrifugation (1300 rpm, 5 min, RT) and the cells were resuspended in 250 μL of Tyrode +2.5 mM CaCl$_2$ and analyzed by flow cytometry. It was considered population events accordingly to Annexin V−/7AAD− (viable cells), Annexin V+/7AAD− (early apoptosis), Annexin V+/7AAD+ (late apoptosis), and Annexin V-/7AAD+ (necrotic death).

2.8. Oxidative Stress. H9c2 cells (7 × 10^4 cells/treatment) were exposed to different concentrations of TiO$_2$ particles (0.01, 0.3, 0.9, 3.1, and 9.4 μg/cm^2) for 24 h. The cellular redox state and oxidative stress were measured by oxidation of either DCFH-DA or MitoSOX. After treatment, cell suspensions were incubated with 0.5 μM DCFH-DA or 5 μM MitoSOX for 15 min at 37 °C. After incubation, cells were washed and analyzed by flow cytometry by measuring the fluorescence of DCFH-DA (E_x = 485 nm; E_m = 530 nm) and MitoSOX (E_x = 510 nm; E_m = 580 nm). At least 10,000 events were analyzed in a FACSCanto II cytometer (BD Biosciences) by triplicates for each set. The samples prepared were not overexposed to light. Finally, the assays were performed in the
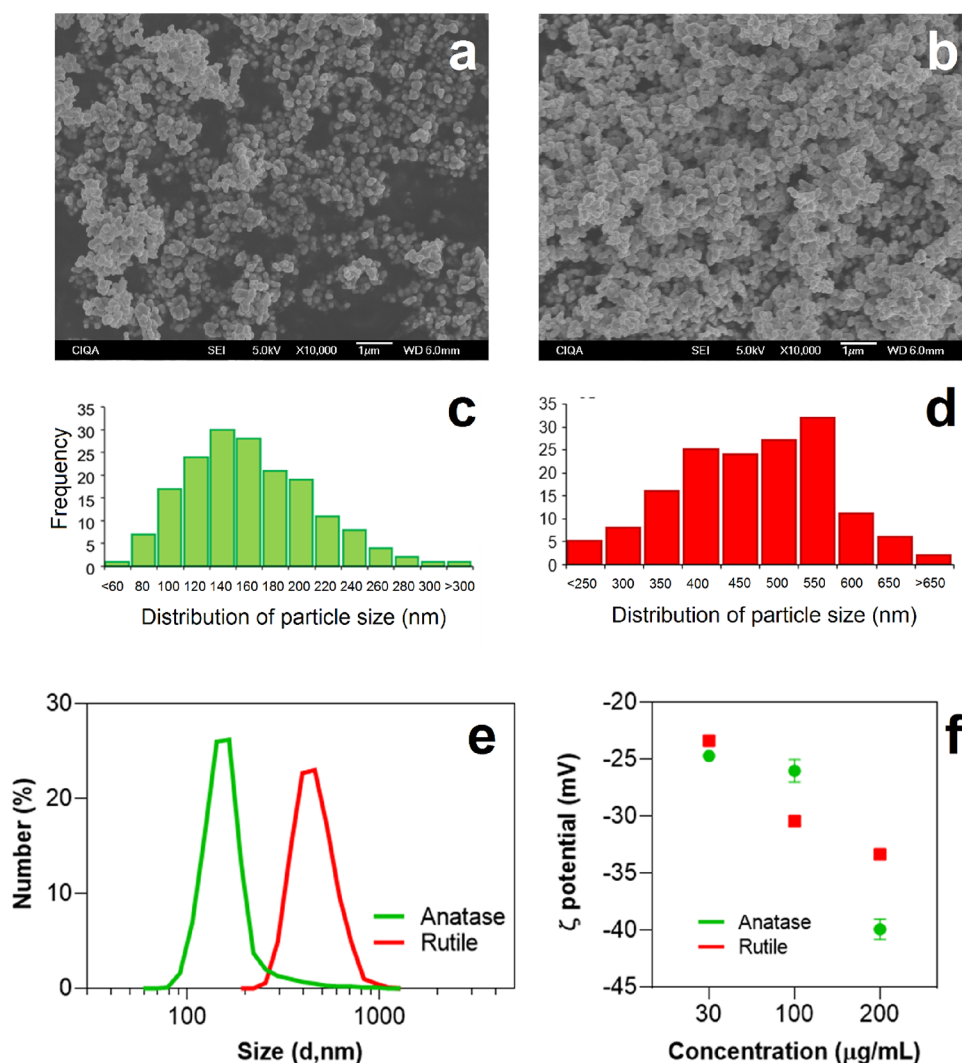
Figure 1. SEM microscopy for TiO$_2$-anatase (a) and TiO$_2$-rutile (b). Particle size distribution by SEM quantification for TiO$_2$-anatase (c) and TiO$_2$-rutile (d). Diameter particle size distribution by DLS (e) and ζ-potential determination for of TiO$_2$-anatase (green points) and TiO$_2$-rutile (red points) dispersed in water at different concentrations (f).

log growth phase, where the cells replicate exponentially with an adequate input of nutrients and space.

2.9. Statistical Analysis. Results are presented as mean ± standard deviation (SD) of at least three independent experiments. ANOVA analyzed mean values, statistical differences, and further multiple comparisons between treatments by Tukey's test. Significance is presented as [a]$p < 0.05$ (treatments versus control) and *$p < 0.05$ for comparisons between particles.
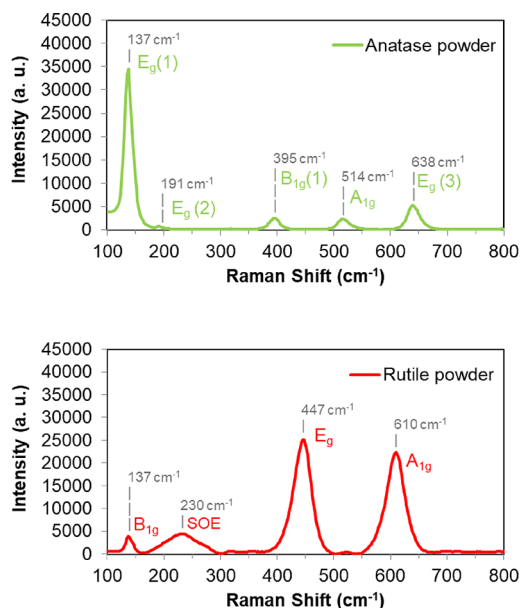
3. RESULTS

3.1. Particle Characterization. TiO$_2$ is mainly prepared as a polycrystalline powder (e.g., anatase, rutile, brookite) using different strategies, precursors, and subsequent treatments[43] that yield distinctive properties for particles. Figure 1 shows the morphology of the particles as analyzed by SEM microscopy. Nearly spherical particle shape and opaque particles appear in the micrographs for TiO$_2$-anatase (see Figure 1a) and TiO$_2$-rutile (see Figure 1b). TiO$_2$-rutile particles appear to be more elongated silhouettes, possibly due to the interface nucleation process and growth during the phase transition.[37] Particle size was estimated by calculating

the visible area and computing the corresponding diameter length considering spherical particles. From microphotographs, the particle sizes for the TiO$_2$ particles are in the submicron range. The particle size distribution (see Figure 1c,d) indicates values that yield a mean of 140 and 450 nm for TiO$_2$-anatase and TiO$_2$-rutile, respectively. Dynamic light scattering measurements estimated the hydrodynamic diameter (see Figure 1e). DLS values calculated for TiO$_2$-anatase and TiO$_2$-rutile were approximately 165 and 468 nm, respectively, in which the TiO$_2$-anatase logarithmic distributions appear with a smaller tail for values less than the mean, overlapping with the TiO$_2$-rutile distribution. The polydispersity index value obtained for anatase is 0.206 ± 0.051, while for TiO$_2$-rutile, it is 0.329 ± 0.089. This result confirms the previous SEM observation in which the particle size distribution is broader for TiO$_2$-rutile.

SEM and DLS measurements indicate that the diameter size for TiO$_2$-anatase and TiO$_2$-rutile is in the same similar particle size range; however, the size distribution is wider for TiO$_2$-rutile and narrower for TiO$_2$-anatase. The ζ-potential was measured at three different concentrations to assess the stability in the media. Figure 1f shows the magnitude of the

ζ-potential. The calculated values for a concentration of 30, 100, and 200 μg/mL are approximately similar for TiO$_2$-anatase (-24.7, -26.0, and -39.9 mV) and TiO$_2$-rutile (-23.3, -30.4, and -33.3 mV). These results indicate that the ζ-potential increases proportionally to the particle concentrations;[44] values greater than +30 mV or less than -30 mV indicate the stability of particle dispersion. It can be observed that the ζ-potential for the particle concentration between 30 and 100 μg/mL typically ranges from -23 to -30 mV. This result suggests that such particle concentrations can be validated for using and controlling the bioassays. For higher concentrations above 100 μg/mL, the particles are susceptible to adhering to one another, forming aggregates, and yielding to sedimentation over time.
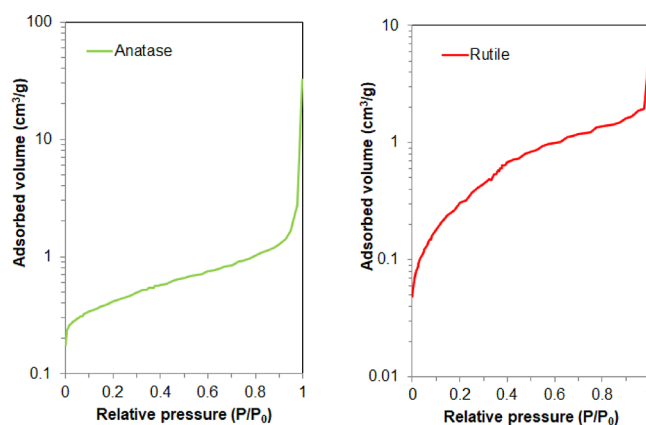
The Raman spectra for TiO$_2$-anatase and TiO$_2$-rutile phases are shown in Figure 2, indicating the main absorptions of each

Figure 3. Nitrogen adsorption isotherms for TiO$_2$-anatase (left, green) and TiO$_2$-rutile (right, red).

observed, leading to a coverage near 1. This result suggests the chemical and geometrical heterogeneity of the surfaces of particles, inducing distinctive interactions between the adsorbate on TiO$_2$-anatase (101) and TiO$_2$-rutile (110) surfaces.[47] For comparison, the Langmuir approximation estimated higher surface areas, namely, 13.1 m^2/g (TiO$_2$-anatase) and 43.1 m^2/g (TiO$_2$-rutile). However, this approximation is often applied when a chemisorbed monolayer is formed or isotherms of type I can describe the physisorption process. For TiO$_2$-anatase, the difference between BET and Langmuir is less than 5 m^2/g, but it is more than 4 times bigger for TiO$_2$-rutile. The measured BET surface areas correlate well with the SEM sizes of about 150 and 440 nm. The calculated parameters are summarized in Table 1.

3.2. Microstructure. Figure 4 shows the powder X-ray diffractograms (XRD) obtained for TiO$_2$-anatase and TiO$_2$-rutile. The diffraction peaks were indexed and compared to the TiO$_2$ patterns (JCPDS cards 21-1272 and 21-1276). XRD confirmed a high degree of crystallinity, as evidenced by the absence of satellite peaks. Table 2 shows the lattice parameters,

Figure 2. Raman spectra of TiO$_2$-anatase (up, green-colored) and TiO$_2$-rutile (down, red-colored).

crystalline phase. Raman analysis confirmed that the surface crystal phase corresponds to the looked-for crystalline phases of TiO$_2$. The observed Raman active modes[45] are E$_g$, A$_{1g}$, and B$_{1g}$. In particular, three bands located at 137, 191, and 639 cm^{-1} are assigned to E$_g$ symmetry for TiO$_2$-anatase. The symmetric stretching vibration of O−Ti−O causes the mode E$_g$, the symmetric bending vibration of O−Ti−O causes the mode B1g, and the mode A$_{1g}$ is caused by the O−Ti−O antisymmetric bending vibration.[46] It has been suggested that the band located at 514 cm^{-1} might be a superposition of A$_{1g}$ and B$_{1g}$ modes as a doublet. Finally, the peak at 395 cm^{-1} (B$_{1g}$ mode) is given by the entire molecule's symmetric folding. Raman active modes in TiO$_2$-rutile appeared at 447 cm^{-1} (E$_g$) and 610 cm^{-1} (A$_{1g}$). A weak peak is at 137 cm^{-1} (B$_{1g}$). The peak located at 229 cm^{-1} is related to the second-order effect due to a multiphonon process of two-photon scattering.[45]

Finally, the surface area was estimated using N$_2$ adsorption (see Figure 3). Type II isotherms were recorded, which are typically obtained for non-porous materials. It was estimated surface areas of about 8.4 and 10.0 m^2/g (multipoint BET) for TiO$_2$-anatase and TiO$_2$-rutile, respectively. For TiO$_2$-rutile, a lower saturation volume in the relative pressure range can be

Table 1. Particle Characterization from SEM, DLS, N$_2$ Adsorption, and X-ray Diffraction Analysis for TiO$_2$-Anatase and TiO$_2$-Rutile Particles

property	TiO$_2$-anatase	TiO$_2$-rutile
particle size (SEM)	151.8 ± 48.6 nm	442.7 ± 100.5 nm
particle size (DLS)	165.5 ± 26.0 nm	468.2 ± 28.5 nm
surface area (BET)	8.40 m^2/g	10.03 m^2/g
surface area (Langmuir)	13.14 m^2/g	43.15 m^2/g
ζ-potential	−24.7 mV (30 μg/mL)	−23.3 mV (30 μg/mL)
	−26.0 mV (100 μg/mL)	−30.4 mV (100 μg/mL)
	−39.9 mV (200 μg/mL)	−33.3 mV (200 μg/mL)
crystallite size (Rietveld)	111.2 ± 2 nm	307.1 ± 1 nm
apparent strain (Rietveld)	0.19%	0.06%
apparent crystallite size (Williamson−Hall)	178.8 ± 18 nm	112.6 ± 20 nm
apparent strain (Williamson−Hall)	0.33%	0.06%
apparent crystallite size (Warren−Averbach)	29.2 ± 3 nm (112)-peak	21.2 ± 2 nm (200)-peak
	43.0 ± 3 nm (224)-peak	18.4 ± 2 nm (400)-peak
apparent strain (Warren−Averbach)	1.02%	0.53%
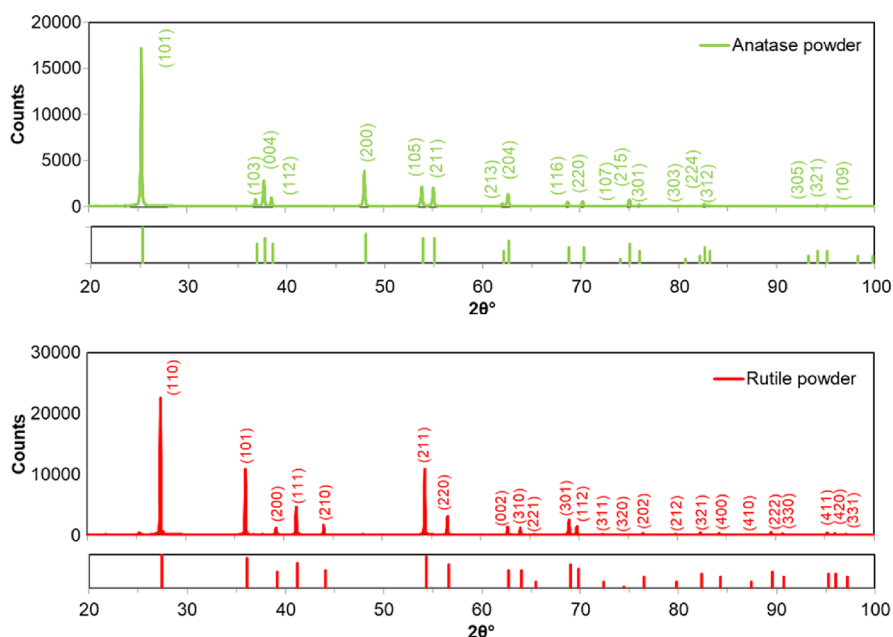
Figure 4. XRD diffractograms for TiO$_2$-anatase (up, green) and TiO$_2$-rutile (down, red). Comparative reflections from the JCPD cards are showed at the bottom.

Table 2. Quantitative Analysis from Rietveld Refinement for TiO$_2$-Anatase and TiO$_2$-Rutile Particles

	phases	composition (%)	GOF	cell parameter (Å)	unit cell volume (Å^3)	occupation of O
TiO$_2$-anatase	anatase	100	1.84	$a = 3.7887(6)$	136.6	$(0, 1/4, z)$
				$c = 9.5221(8)$		$z = 0.1686(2)$
TiO$_2$-rutile	rutile	98.85	2.49	$a = 4.5949(5)$	62.5	$(x, x, 0)$
				$c = 2.9597(1)$		$x = 0.3060(5)$
	anatase	1.15		$a = 3.7860(4)$	136.4	$(0, 1/4, z)$
				$c = 9.515(2)$		$z = 0.166(6)$

crystallite size, and microstrain obtained from Rietveld analysis. The qualitative phase analysis was performed using the TOPAS software. It was determined that the TiO$_2$-anatase particles were 100% of the anatase phase, while the TiO$_2$-rutile particles were 98.85% rutile and 1.15% anatase. For TiO$_2$-anatase, the values $a = 3.7878$ Å and $c = 9.5221$ Å were obtained. These values are comparable to others studies that determined by several techniques minimal variations of TiO$_2$-anatase lattice parameters as a function of particle size.[48,49] For TiO$_2$-rutile, the lattice parameters $a = 4.5949$ Å and $c = 2.9597$ Å were obtained, which are similar to values previously reported[40] for rutile obtained from calcination processes. Additionally, the crystallite size was estimated at 111 and 307 nm, for TiO$_2$-anatase and TiO$_2$-rutile, respectively. Comparison with SEM and DLS measurements indicate that the TiO$_2$-anatase particles comprised one crystallite. At the same time, the structure of TiO$_2$-rutile might be constituted by some crystallites ($\sim$4) aggregated into particles with a large polycrystalline nature, probably due to the heat treatment for obtaining the rutile TiO$_2$ phase. Moreover, the presence of microstrain was estimated at 0.19% and 0.06%, for TiO$_2$-anatase and TiO$_2$-rutile, respectively.

X-ray line profile analysis was carried out through the WH and WA methods. The crystallite size and microstrain were evaluated from the diffraction peaks broadening.[38] The Williamson–Hall plots are shown in Figure 5. An apparent crystallite size for TiO$_2$-anatase was estimated at 179 nm, while the apparent microstrain was calculated at 0.33%. For TiO$_2$-

rutile, the crystallite size was calculated at about 110 nm with a 0.06% for microstrain. Notably, the crystallite size values are similar to those obtained from the Scherrer analysis and SEM. The presence of microstrain contribution is more significant in TiO$_2$-anatase. It can be ascribed to typical microstructure from crystal defects or dislocations located at the surface of particles.[50] Likewise, the microstrain in TiO$_2$-rutile particles suggests the presence of dislocations and other crystal defects. For comparison, the Warren–Averbach analysis for TiO$_2$-anatase and TiO$_2$-rutile[40] was used to estimate the apparent crystallite size. The natural logarithm of the size coefficient A^s (L) for the $\langle 112 \rangle$ and $\langle 200 \rangle$ family planes yield smaller crystallite sizes of approximately 29 nm and 21 nm for TiO$_2$-anatase and TiO$_2$-rutile, respectively. The data points reveal a certain degree of microstrain, which is more significant in TiO$_2$-anatase as compared to TiO$_2$-rutile, $\langle \varepsilon^2 \rangle = 1.02\%$ and $\langle \varepsilon^2 \rangle = 0.53\%$, respectively. The effect of microstrains on the properties of TiO$_2$ particles can influence the catalytic and photocatalytic performance and determines their adsorption capacity.[50]

3.3. Metabolic Activity and Membrane Integrity. The H9c2 cell metabolic viability was evaluated in a dose-dependent manner. The cell death was examined after 24 h of treatment from seeding with particles. Figure 6a depicts the cellular viability percentage using the Alamar Blue (AB) assay, which is a fluorescent indicator dye that detects oxidation levels during respiration by all the components of the electron transport chain.[51] A drop in intensity by fluorescence indicates
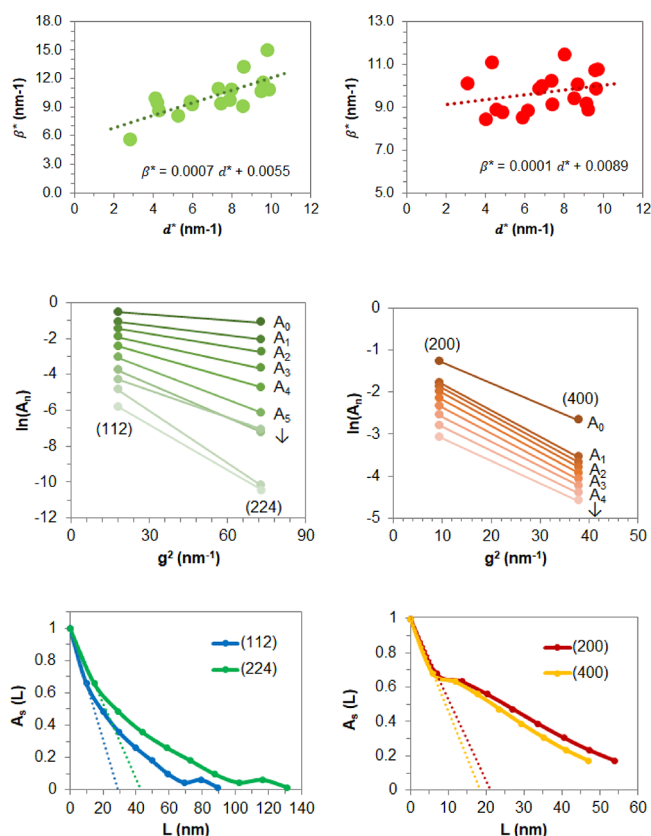
Figure 5. Crystallite size analysis from Williamson−Hall line fitting (top) and Warren−Averbach plots (middle and bottom) in TiO$_2$-anatase (left) and TiO$_2$-rutile (right) particles.

that cellular activity decreases as long as the concentration of particles increases. In particular, the effects induced by TiO$_2$ on the metabolic activity of H9c2 cells become apparent at concentrations from 3.12 μg/cm^2 (equivalent to 10 μg/mL). Incubation of H9c2 myoblasts with either TiO$_2$-anatase or TiO$_2$-rutile particles induces pronounced cell viability loss (>50%) and probably cell death, especially at concentrations higher than such concentration. In comparison, a low viability loss (<25%) occurs at the lowest concentrations analyzed (<0.9 μg/cm^2). A direct visualization of the dose−response curves suggested different mechanisms of association between cells and particles. For instance, the curve for TiO$_2$-anatase showed a higher degree of sensitivity (i.e., Hill slope) at the lowest concentrations. However, TiO$_2$-rutile appeared to be more reactive at the highest concentrations. These observations suggested that the association between TiO$_2$-rutile particles and H9c2 cells occurred at a low extent as compared to TiO$_2$-anatase (*p < 0.05). The distinctive association between cells and particles can be attributed to the particle size; from Rietveld analysis, a 4-fold shorter size for TiO$_2$-anatase (150 nm) compared to TiO$_2$-rutile (440 nm) was estimated. The cytotoxic effect induced from nanosized TiO$_2$ particles is generally ascribed to the dissociative adsorption of water into OH$^\bullet$ at the titania surfaces, while TiO$_2$, in its submicron-scale form, is considered generally inert.[25]

Table 3 shows the resulting Tukey post hoc test from the one-way ANOVA. The inhibitor concentration IC$_{50}$ was estimated from the normalized response described by the Hill−Langmuir equation. The individual t test analysis for the IC$_{50}$ resulted in 9.35 μg/cm^2 (29.9 μg/mL) and 7.92 μg/cm^2

(25.4 μg/mL) for TiO$_2$-anatase and TiO$_2$-rutile, respectively. These IC$_{50}$ values are approximately 2-fold lower (20 μg/cm^2) compared with other reports[24] that evaluated the metabolic viability of TiO$_2$-anatase in H9c2 cardiomyoblasts. Interestingly, at the IC$_{50}$, the t test analysis showed that the metabolic activity of TiO$_2$-anatase is not different than TiO$_2$-rutile (*p > 0.05). At the IC$_{25}$, the ANOVA analysis showed (*p value, 0.14) that the metabolic activity of TiO$_2$-anatase (1.4 μg/cm^2 equivalent to 4.6 μg/mL) is also not different than TiO$_2$-rutile (4.4 μg/cm^2 equivalent to 14.1 μg/mL). It can be suggested that the two TiO$_2$ particles produced similar loss of metabolic activity at the IC$_{25}$ and IC$_{50}$ concentrations, despite their differences in the particle size and other characteristics, such as the crystalline phase. A previous report by Huerta-García and collaborators[24] indicated that TiO$_2$-anatase particles 20 μg/cm^2 (100 μg/mL) induced a cell viability loss in 50%. Inhibitory concentrations were also computed for IC$_{75}$. However, the potency of TiO$_2$ particles in inhibiting metabolic activity at such concentration suggests that TiO$_2$-anatase and TiO$_2$-rutile possess differential reactivity toward H9c2 cardiomyoblasts (*p < 0.05). In this case, the IC$_{75}$ values suggested that TiO$_2$-rutile (23.1 μg/cm^2 equivalent to 74 μg/mL) can cause an exacerbation in the cytotoxicity of H9c2 cells regarding TiO$_2$-anatase (123.4 μg/cm^2 equivalent to 395 μg/mL). Based on our results, it is suggested that H9c2 cardiomyoblasts are also susceptible to TiO$_2$-rutile particles, which can induce a cell viability loss in a large extent of 75%, at moderate concentrations (∼20 μg/cm^2) similar to TiO$_2$-anatase particles as shown by others.[24]

Figure 6b shows the evaluation of membrane integrity using particle concentrations lower than the IC$_{50}$ value. It was measured in a dose-dependent manner after 24 h. Fluorometric tests for Annexin V and 7-AAD were analyzed by flow cytometry accordingly to previous studies.[51] A direct interaction between titania and reagents might cause artifacts; however, our assays indicated that neither Annexin V nor 7-AAD interacted with particles (data not shown). Moreover, the ANOVA analysis showed a statistical difference (*p < 0.05) compared with untreated cells. Previous reports[21] have suggested that food-grade TiO$_2$ particles at concentrations of about 20 μg/cm^2 (100 μg/mL) disrupted the plasmatic membrane integrity leading to high levels of permeability. From Figure 6b, it can be observed that at the lowest concentrations (<0.9 μg/cm^2), the membrane integrity is not severely compromised (∼10%) when H9c2 cells interacted with either TiO$_2$-anatase or TiO$_2$-rutile particles. However, it seems that the membrane integrity can be a barely dependent variable (*p < 0.05) for the type of particle at concentrations of about 3 μg/cm^2 and higher. The membrane integrity loss due to interaction with TiO$_2$-rutile particles is about 30%. In comparison, H9c2 cells interacting with TiO$_2$-anatase compromised the integrity of the cell membrane in about 50%. These findings highlight that titania can induce distinctive membrane associations with TiO$_2$-anatase and TiO$_2$-rutile particles despite the fact that the two type of particles induced similar cellular viability. Based on the assessment of cell viability loss and membrane integrity, we suggested that H9c2 cardiomyoblasts can also be associated with TiO$_2$-rutile particles when concentrations are about the inhibitory concentration IC$_{50}$.

3.4. Apoptosis and Necrosis Cell Death Events. Apoptotic (Figure 6c,e) and necrotic (Figure 6d,f) death events in H9c2 cardiomyoblast were inferred from the staining
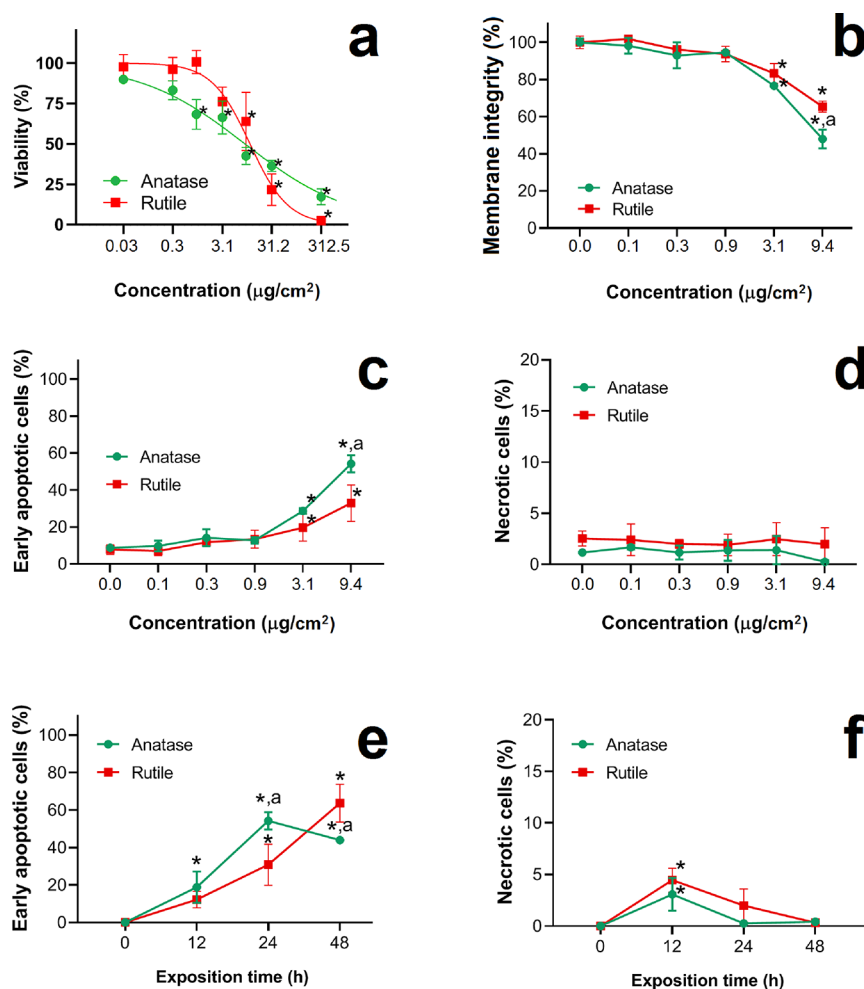
Figure 6. Dose-dependent viability and cell death events after 24 h. (a) Dose-dependent metabolic activity; (b) dose-dependent cells permeability; (c) early apoptotic cells; (d) necrotic cells. Time-dependent cell death using the particle concentration at the IC_{50} for anatase and rutile. (e) Early apoptotic cells; (f) necrotic cells. Data are presented as mean $\pm$ SD, $n = 5$, statistical difference [a]$p < 0.05$ vs untreated cells, and *$p < 0.05$ anatase vs rutile.

Table 3. Inhibitory Concentrations for TiO$_2$ Particles Are Indicated in μg/cm^2 (Values in Parenthesis Are Equivalents in μg/mL)[a]

	IC_{25}	IC_{50}	IC_{75}
TiO$_2$-anatase	1.44 $\pm$ 1.2 (4.60 $\pm$ 3.9)	9.35 $\pm$ 0.8 (29.91 $\pm$ 2.8)	123.49 $\pm$ 1.1 (395.19 $\pm$ 3.5)
TiO$_2$-rutile	4.41 $\pm$ 1.4 (14.10 $\pm$ 4.4)	7.92 $\pm$ 0.9 (25.36 $\pm$ 3.08)	23.09 $\pm$ 0.9 (73.91 $\pm$ 2.88)
*p value	0.14	0.06	0.04

[a]Statistical analysis indicates moderate evidence suggesting that the evaluated metabolic viability of TiO$_2$-anatase in cardiomyoblasts is not different than TiO$_2$-rutile for the IC_{25} and IC_{50}. However, the cell viability loss can be differentiated at the IC_{75} (*$p < 0.05$).

observed using Annexin V and 7AAD, in dose-dependent and time-dependent measurements. In general, apoptosis events (Annexin V+/7AAD−) generated by titania appeared at the lowest concentrations (<1 μg/cm^2) for a dose-dependent treatment (at 24 h), and such events increase as long as the concentration of particles increases. However, the ANOVA analysis suggested moderate evidence (*$p < 0.05$) that the early apoptotic events can be when concentrations of particles are above 3 μg/cm^2. Our results estimated that TiO$_2$-anatase

induces a double amount of events ($\sim$60%) compared to TiO$_2$-rutile particles at a concentration of about 9.4 μg/cm^2.

Figure 6d shows the necrosis death events (Annexin V−/7AAD+) evaluated after 24 h. It can be observed that the percentage of necrotic cells is minimal (<3%) and similar for the two types of particles. The low incidence of necrotic cell death suggests that this type of cell death may not play a significant role in the toxicity of TiO$_2$ particles in H9c2 cells. In comparison, previous studies[21] reported that food-grade TiO$_2$ (i.e., anatase) particles produced a significant increase in necrotic cell death but minimal apoptosis. It is important to note that early apoptotic events are not necessarily indicative of cell death, but rather a response to stress that can potentially be reversed. Previous studies[36] revealed that TiO$_2$-anatase and TiO$_2$-rutile particles had distinct abilities to associate to the membrane,[36] which might imply different mechanisms for internalization and further cell death. Apoptotic events may be the main mechanism of cell death only upon long-term exposures and probably after particle internalization.

Time-dependent cell death events were evaluated after treatment with TiO$_2$ particles at 0, 12, 24, and 48 h. Early apoptosis (see Figure 6e) and necrosis events (see Figure 6f) were measured at the IC_{50} values calculated for TiO$_2$-anatase (9.4 μg/cm^2) and TiO$_2$-rutile (7.9 μg/cm^2). The apoptosis
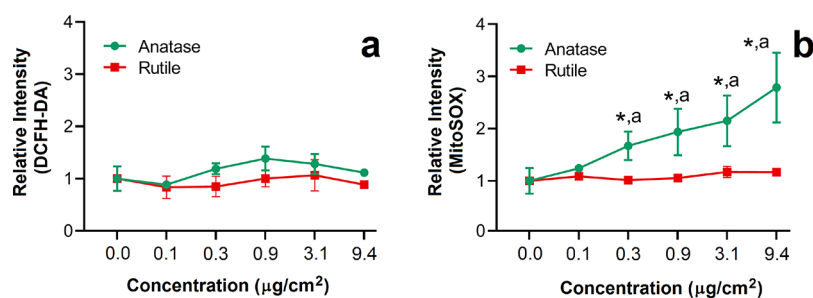
Figure 7. Cellular redox state in a dose-dependent treatment. (a) Intracellular ROS production as evaluated by DCFH-DA oxidation; (b) mitochondrial ROS production as evaluated by MitoSOX oxidation. Data are presented as fluorescence relative intensity units regarding the control group. Mean $\pm$ SD, $n = 4$, $^a p < 0.05$ vs untreated cells, and $^* p < 0.05$ anatase vs rutile.

observed seems to increase quite regularly during the exposition time for TiO$_2$-rutile particles. For instance, the influence of apoptotic events at 48 h appeared to be approximately 50%. It is evident that either TiO$_2$-anatase or TiO$_2$-rutile particles can activate early apoptosis after prolonged exposures (>24 h). The estimated statistical difference ($^* p$ value, 0.045) suggest that there are no significant differences between the TiO$_2$-anatase and TiO$_2$-rutile particles. Finally, in agreement with the dose-dependent results, the relative percentages for necrosis events are similar for the two types of particles (<3%). TiO$_2$ particles barely induced cell death by necrosis, even at extended periods. The time-dependent changes observed in the induction of early apoptosis events may be related to extracellular association with particles. The formation of intracellular and extracellular ROS[24,28] when the H9c2 interacted with TiO$_2$ particles is examined in the following section.

3.5. Reactive Oxygen Species Production. The oxidant-generating potential in a cell-free medium can be utilized as a pre-screening method to assess the reactivity of TiO$_2$ particles based on their physicochemical properties. In a study conducted by Huerta-Garcia et al.,[24] the cellular redox state and ROS production were measured using the DCFH-DA assay. Results showed that TiO$_2$-anatase strongly increased the fluorescence intensity by 17-fold, in direct proportion to DCFH-DA oxidation (refer to Figure 7a,b). In evaluating the effect of TiO$_2$ particles on H9c2 cardiomyoblast cells, DCFH-DA oxidation revealed no significant differences between the treatment and control groups. The highest observed effect was a mere 20% increase in fluorescence intensity with TiO$_2$-anatase particles at a concentration of 0.9 μg/cm^2. It is worth noting that DCFH-DA is a cell-permeable ester that can be hydrolyzed inside the cell to form dihydroxy-DCFH. Consequently, DCFH does not directly react with H$_2$O$_2$, and the current assays may artificially quantify ROS overproduced by the oxidation of DCFH to DCF, which produces superoxide. Therefore, the specificity of the DCFH-DA assay in measuring the overall cellular redox state is unclear as it could be both intracellular and mitochondrial.[52] Moreover, the DCFH-DA assay revealed that TiO$_2$-rutile particles were unable to generate ROS, consistent with previous findings by other researchers.[53]

In order to further investigate the generation of ROS, we utilized the MitoSOX-based assay, as shown in Figure 7b. This assay has been previously used[11,21,32] as an indicator of perturbation of TiO$_2$ particles in mitochondrial dynamics and is commonly used[54] for the selective detection of mitochondrial superoxide in living cells. Our results indicated that exposure of H9c2 cells to TiO$_2$-anatase significantly increased

mitochondrial ROS production for all evaluated concentrations. Specifically, the highest effect was observed for TiO$_2$-anatase particles at a concentration of 0.9 μg/cm^2, resulting in a 100% increase ($^* p > 0.05$) in ROS production compared to control cells or TiO2-rutile particles. Interestingly, incubation of H9c2 cells with TiO$_2$-rutile resulted in the absence of ROS formation. Thus, TiO$_2$-rutile particles appear to be incapable of producing superoxide species. These results suggest two key points: first, TiO$_2$-rutile particles may not be able to internalize into cells to induce alterations in cellular mechanisms via mitochondria; second, TiO$_2$-anatase particles may be internalized and interact with the respiratory chain complex, modulating ROS generation. Overall, these findings suggest that differences in particle characteristics induce distinctive interactions with cells, leading to differential associations with the cellular membrane (see Section 3.3).

4. DISCUSSION

A clinical association between exposures to particulate matter has been correlated with a risk of cardiovascular diseases, such as hypertension, myocardial infarction, and heart failure.[11−13,16,55,56] It is also suggested that TiO$_2$ particles cannot penetrate through slightly damaged skin caused by applied products in vivo.[14] However, TiO$_2$ particles were found in the plasma and urine of humans after 6 h of sunscreen use.[15] In particular, TiO$_2$ particles exposed directly to cell culture in vitro significantly affect cell viability.[20,21,23,24,30] The potential cytotoxicity of TiO$_2$ particles observed for different biological models is still an open question regarding the effect on cardiac cells.

Toxicological assessments of particles typically rely on physical−chemical characteristics, such as size, shape, crystal structure, degree of crystallinity, and coating or additional chemical surface treatments.[6,23,26−28,31,33,35,53] While cytotoxicity studies are often carried out using the phase TiO$_2$-anatase, there remains significant heterogeneity in determining the cytotoxic effects solely to the crystalline phase.[23,26,28,33,53] Despite this, Hattori et al.[26] suggested that the crystalline phase of titania has a more significant effect on cellular absorption than particle size. Particularly, in the case of food-grade titania particles (i.e., TiO$_2$-anatase), cardiovascular effects[17,21,24] and cytotoxicity appear less severe[24] at concentrations lower than 20 μg/cm^2. Interestingly, some reports[35,36] have shown that the phase TiO$_2$-anatase does not always induce the highest toxicity. For example, Katsumitti et al.[22] demonstrated low and dose-dependent toxicity in mussel hemocytes and gill cell models, suggesting that a mixture of anatase/rutile produces more toxic effects than pure TiO$_2$-

anatase. Similarly, Hussain and collaborators[28] evaluated the crystalline phase as the mediating property for TiO_2 toxicity using the HEL-30 mouse keratinocyte cell line model and found that TiO_2-rutile initiated apoptosis by forming reactive oxygen species (ROS). In other studies, Yu et al.[36] also indicated that TiO_2-anatase might pose lower toxicity against macrophages than TiO_2-rutile.

In the case of TiO_2-anatase particles, a direct correlation between the crystalline phase and cytotoxicity presents conflicting views from the cell death mechanisms.[22,26,28,33] TiO_2-anatase is generally considered to be 100 times more toxic than TiO_2-rutile in the submicron range.[18,23,25] However, in vitro studies[28,36] have suggested that TiO_2-rutile may pose higher toxicity than TiO_2-anatase due to its distinctive associativity with phospholipids in the cell membrane. This observation is supported by others[28] pointing out that TiO_2-rutile particles can also generate high ROS levels.[47] Currently, in vitro evaluations have not yielded conclusive data to determine whether TiO_2-rutile particles can mediate cytotoxicity in cardiomyoblasts. In this work, we showed moderate evidence (*$p < 0.05$) that the integrity of the cell membrane remained similar for either TiO_2-anatase or TiO_2-rutile at the inhibitory concentrations IC_{25} and IC_{50}. However, it is important to note that the potential toxicological risk of TiO_2-rutile at higher inhibitory concentrations deserves special attention. At such concentrations (i.e., IC_{75}), the cell viability loss induced by TiO_2-rutile is more evident than that induced by TiO_2-anatase. We observed that the cytotoxic effects on the membrane integrity due to the association with TiO_2-rutile particles appeared to exacerbate at concentrations not considered critical ($\sim$20 $\mu g/cm^2$). However, severe exposure (>100 $\mu g/cm^2$) to TiO_2-anatase particles is required to induce a similar percentage of cell viability loss. These results indicate that TiO_2-rutile particles may also be cytotoxic in H9c2 cardiomyoblasts, in which morphological alterations at the membrane may be primarily attributed to particle association. It is well-known that TiO_2 particles can induce morphological changes that substantially induce cell death. For example, in A549 cells, the cell viability loss (>25%) was reported[35] to follow endocytic internalization processes and decrease in a dose-dependent manner. Interestingly, we also observed that after 24 h of exposure, the extent of cell damage increased (i.e., membrane integrity loss >70%), making it difficult to evaluate internalization and cytoplasmic accumulation of TiO_2 particles. Overall, it is difficult to evaluate internalization and cytoplasmic accumulation of TiO_2 particles.

The mechanism of cell death induced by TiO_2-anatase and TiO_2-rutile is likely almost similar in terms of metabolic inhibition (see Figure 6a), membrane integrity (see Figure 6b), and necrosis (see Figure 6d,f) for a concentration of about the IC_{25} and IC_{50}. However, it was observed distinctive effects in terms of apoptosis (see Figure 6c,e) and production of mitochondrial ROS (see Figure 7). A distinction in cell injury by TiO_2 particles was observed in terms of apoptotic events and mitochondrial ROS production. Our results indicated that TiO_2-rutile particles induce less early apoptotic events than TiO_2-anatase particles (*$p < 0.05$), although neither of the particles induced necrosis. These findings suggest that TiO_2-anatase and TiO_2-rutile particles may have different cellular toxicity mechanisms. Previous studies[24,26,32] have suggested that the toxicity of TiO_2 particles may be related to ROS production, accumulation, and deficiency of antioxidant defense. TiO_2 particles might induce tissue damage and

inflammatory responses; however, the underlying mechanisms are not well understood in the cardiovascular system. It is believed[24] that the presence of TiO_2 particles can induce morphological changes related to increased numbers of cell vacuoles that trigger autophagy and oxidative stress, which could be the primary mechanism for TiO_2 NP toxicity in cardiomyoblasts. In our study, we observed that both TiO_2-anatase and TiO_2-rutile particles could trigger a loss of cell viability and early apoptosis events at low concentrations of particles ($\sim$3 $\mu g/cm^2$). TiO_2-anatase was found to significantly increase ROS produced at the mitochondrial level, while TiO_2-rutile appeared to be inefficient in producing superoxide species, suggesting that TiO_2-rutile may be unable to undergo internalization due to the formation of large aggregates. Our findings suggest that TiO_2-anatase and TiO_2-rutile particles induce similar toxicity at concentrations close to the IC_{25} and IC_{50}, but under different mechanisms. TiO_2-anatase is capable of increasing mitochondrial ROS, while TiO_2-rutile seems to be inefficient in producing superoxide species.

Interestingly, we found that both crystalline phases had a similar IC_{50}, as evidenced by the production of reactive oxygen species (ROS). Our results also indicated the absence of changes in the cellular redox state (see Figure 7a), suggesting that that neither phase significantly modified the cellular ROS. Our results based on DCFH-DA assays indicated a minimal production of ROS, suggesting that the origin of cell damage might be intracellular for TiO_2-anatase or extracellular for TiO_2-rutile. The samples were not overexposed to light to avoid activation and interference with particles and fluorophores in all experiments. To further understand the mechanism of toxicity, we used the MitoSOX-based assay to identify the generation of ROS from mitochondria, which can be a significant source of cellular superoxide. We observed that TiO_2-anatase induced a three-fold increase in mitochondrial superoxide production, suggesting a potential association with the membrane, occurrence of internalization processes, and interactions with mitochondria. This observation is consistent with previous reports,[24] indicating that TiO_2-anatase can ameliorate the mitochondrial membrane potential after internalization into the cytoplasm of H9c2 rat cardiomyoblasts. In contrast, incubations of H9c2 cells with TiO_2-rutile led to the null formation of ROS. This finding suggests that TiO_2-rutile might be unable to undergo internalization due to the formation of large aggregates, yielding a high cell viability loss (IC_{75}). Overall, our results suggest that TiO_2-anatase and TiO_2-rutile particles induced similar toxicity (IC_{25} and IC_{50}) but under different mechanisms. Anatase is capable of increasing mitochondrial ROS, but neither significantly modifies cellular ROS, while the evidence for the role of the crystalline phase TiO_2-rutile requires further evaluations to highlight potential health effects regarding association and internalization processes in cardiomyoblasts.

The particles were characterized for their pure crystalline phases, surface areas, and ζ-potential values, and the results are presented in Tables 1 and 2. It is plausible that the heterogeneity along the surfaces of TiO_2 particles might induce distinctive interactions with adsorbates. The superior photocatalytic activity of TiO_2-anatase particles cannot be solely attributed to the typically larger surface areas found in anatase, but rather to the fundamental differences between the anatase and rutile surfaces.[25] TiO_2-anatase with high-energy facets has a higher adsorptive affinity and is less thermodynamically stable.[57] This property can be associated with the

critical role of {100} facets, which exhibit higher catalytic activity than {101} facets.[57,58] Consequently, particles with a large density of {100} facets can significantly enhance reactivity compared to particles with a large volume of {101} facets. From XRD measurements, it is observed that TiO_2-rutile possesses a similar presence of (101) planes compared to TiO_2-anatase. However, TiO_2-anatase has a four-fold increase in the presence of {100} facets allocated in a comparable surface area (~ 10 m^2/g). Our results show that microstrain contributions are more significant in TiO_2-anatase (1.02%, WA; 0.33% WH) compared to TiO_2-rutile (0.53%, WA; 0.06% WH). Thus, a typical microstructure due to the presence of crystal defects or dislocations located at the surface of TiO_2 particles can enhance high levels of photoreactivity. Recent studies[50] suggested that microstrains can be associated with enhancing the catalytic and photocatalytic performance of TiO_2 particles. Hence, the significant reactivity in the (101) surfaces might trigger the formation of hydrogen bonds[47] with components allocated into the membrane (e.g., proteins and phospholipids). Although the effects of microstrain on the adsorption capacity of TiO_2 particles are yet to be fully established in H9c2 cardiomyoblasts, we believe that the biological responses can be associated only with the characteristics of particles. First, the in vitro experiments avoided the exposure to light for longer periods. Second, the cell cycle was not manipulated, and it ensured asynchronous and homogeneous cycling. Thus, the assays were performed in the log growth phase, where the cells replicate exponentially, and hence, the cell cycle does not become a determining factor. We suggest that the ability of TiO_2 particles to induce cytotoxicity in H9c2 cardiomyoblasts can be related to three main factors: (i) the degree of microstructure to enhance adsorptive processes,[50] (ii) the crystalline phase to induce distinctive interactions at the membrane with proteins and phospholipids,[33,36] and (iii) the size of particles to facilitate internalization.

TiO_2 particles have unique properties such as high surface area, photocatalytic activity, and biocompatibility that make these particles a promising material for a wide range of applications. In healthcare, for instance, TiO_2 particles have been studied for their potential as drug delivery vehicles, wound healing agents, and imaging agents.[7] TiO_2 particles can be functionalized with drugs, peptides, and other biomolecules to target specific cells or tissues, and their photocatalytic activity can also enhance the therapeutic effects of some drugs. In wound healing, TiO_2 particles can promote tissue regeneration and reduce the risk of infection. In imaging, TiO_2 particles can enhance the contrast of MRI and X-ray imaging, enabling the visualization of tissues and organs with greater clarity. The potential health effects of TiO_2 particles would guide strategies for market adoption.

The use of TiO_2 particles in the biomedical field requires careful consideration of their limitations. One of the primary concerns is their size-dependent toxicity, as titania particles can penetrate biological barriers and accumulate in organs and tissues, leading to adverse effects.[11] Furthermore, the limited bioavailability of TiO_2 particles due to their tendency to form aggregates in biological fluids is another challenge to their biomedical applications. Long-term exposure to TiO_2 particles, especially in patients with pre-existing diseases,[13,19,56] also raises concerns regarding their safety. Another challenge to the use of TiO_2 particles in the biomedical field is the scalability and reproducibility of their synthesis and manufacturing. The

production of particles on a large scale and with consistent quality remains a challenge,[7] which limits their use in different laboratories and may compromise protocol standardization.

In this study, we chose to use H9c2 rat cardiomyoblasts as a model system for evaluating the toxicity of TiO_2 particles. The extent to which H9c2 cells can accurately mimic the hypertrophic responses of primary cardiac myocytes was recognized by others,[34] showing identical hypertrophic responses to those observed in primary cardiomyocytes. This finding validated the importance of H9C2 cells as a model for in vitro studies of cardiac hypertrophy. The cytotoxicity effects of TiO_2 in the cardiovascular system was recently described by others[21,24] using H9c2 cells. The potential health risks associated with the exposure of other particles (e.g., SiO_2 and graphene oxide) to H9c2 cells[59,60] was described previously. In particular, H9c2 cells were used in vitro to study particle cytotoxicity[60] and cardioprotective interventions due to their phenotypic and biochemical similarities with mature cardiomyocytes.[59] This way, H9c2 cells offered several advantages such as easy handling, low cost, and reproducibility, making them an excellent choice for our study.

However, it is also important to recognize experimental limitations. First, the use of cell lines, such as H9c2 rat cardiomyoblasts, can further complicate the interpretation of results. These cell lines are immortalized and may not accurately reflect the behavior of primary cells in vivo. Additionally, the conditions under which these cells are grown and maintained in the laboratory may differ significantly from the in vivo environment, which can affect their responses to stimuli. While these studies can provide valuable insights and generate hypotheses for further investigation, it is important to validate these findings using in vivo models.[9,12,13,19] However, there are several reasons why in vivo models may also not be fully representative of human physiology, including species-specific differences in the structure and function of the cardiovascular system. For example, the size and shape of the heart as well as the number and distribution of blood vessels can vary between species. Additionally, the genetic and environmental factors that influence cardiovascular health may differ between normal and hypertensive animals.[13,19] Therefore, a comprehensive understanding of the potential health risks associated with TiO_2 exposure requires a multidisciplinary approach. We recognize this limitation in the current study and highlight the need for further research.

5. CONCLUSIONS

In vitro cytotoxicity assays demonstrated that TiO_2-anatase or TiO_2-rutile particles pose a similar potential risk at the inhibition concentrations of IC_{25} and IC_{50}. Viability and membrane integrity assays also suggested that toxicity in H9c2 cells is time-dependent when exposed to prolonged exposures of about 24 h. Our findings showed that the cytotoxic effects induced apoptosis, while necrosis events were not observed at the concentration of particles used in the study. Furthermore, the production of intracellular ROS had no significant relevance for either TiO_2-anatase or TiO_2-rutile. However, the cellular redox state analysis revealed that the exposure of H9c2 cells to TiO_2-anatase significantly increased mitochondrial ROS production in a dose-dependent manner. Conversely, incubations of H9c2 cells with TiO_2-rutile led to the null formation of mitochondrial ROS. Interestingly, the H9c2 cardiomyoblasts exhibited differential toxicological suscepti-

bility at higher inhibitory concentrations, where TiO_2-rutile induced a severe cell viability loss, likely due to extracellular damage and potential association with the membrane. The morphological and structural characterization of TiO_2 particles has revealed fundamental differences in crystalline phase, microstructure, and particle size, which might induce distinctive interactions with H9c2 cells. In particular, our results indicated that microstrain contributions are more significant in TiO_2-anatase than TiO_2-rutile, suggesting that the presence of crystal defects can enhance the reactivity of particles. Interestingly, the cellular redox state suggested that TiO_2-anatase significantly increased mitochondrial ROS production, while TiO_2-rutile particles induced a null response. The particle size might also contribute to differentiating the association with cells. However, the mechanisms of internalization of TiO_2 particles in myocardial cells merit further investigation.

■ AUTHOR INFORMATION

Corresponding Authors

Gerardo de Jesús García-Rivas − *Escuela de Medicina y Ciencias de la Salud, Tecnologico de Monterrey, Monterrey, N.L. 64460, Mexico; The Institute for Obesity Research, Tecnologico de Monterrey, Monterrey, N.L. 64849, Mexico;* Email: gdejesus@tec.mx

Flavio F. Contreras-Torres − *Escuela de Ingeniería y Ciencias and The Institute for Obesity Research, Tecnologico de Monterrey, Monterrey, N.L. 64849, Mexico;* ⊙ orcid.org/0000-0003-2375-131X; Email: contreras.flavio@tec.mx

Authors

Pamela Santos-Aguilar − *Escuela de Ingeniería y Ciencias, Tecnologico de Monterrey, Monterrey, N.L. 64849, Mexico*

Judith Bernal-Ramírez − *Escuela de Medicina y Ciencias de la Salud, Tecnologico de Monterrey, Monterrey, N.L. 64460, Mexico*

Eduardo Vázquez-Garza − *Escuela de Medicina y Ciencias de la Salud, Tecnologico de Monterrey, Monterrey, N.L. 64460, Mexico*

Lydia Yerid Vélez-Escamilla − *Escuela de Ingeniería y Ciencias, Tecnologico de Monterrey, Monterrey, N.L. 64849, Mexico*

Omar Lozano − *Escuela de Medicina y Ciencias de la Salud, Tecnologico de Monterrey, Monterrey, N.L. 64460, Mexico; The Institute for Obesity Research, Tecnologico de Monterrey, Monterrey, N.L. 64849, Mexico*

Complete contact information is available at:
https://pubs.acs.org/10.1021/acsomega.3c01771

Author Contributions

P.S.-A.: methodology, formal analysis, investigation, writing−original draft. E.V.-G.: methodology, formal analysis, investigation. J.B.-R.: validation. L.V.-E.: methodology, investigation. O.L.: investigation, validation. G.G.-R.: conceptualization, validation, resources, writing−review & editing, project administration, funding. F.F.C.-T.: conceptualization, methodology, validation, resources, writing−original draft, writing−review & editing, supervision.

Notes

The authors declare no competing financial interest.

■ ACKNOWLEDGMENTS

■ REFERENCES

(1) Hext, P. M.; Tomenson, J. A.; Thompson, P. Titanium dioxide: Inhalation toxicology and epidemiology. *Ann. Occup. Hyg.* **2005**, *49*, 461−472.

(2) Fei Yin, Z.; Wu, L.; Gui Yang, H.; Hua Su, Y. Recent progress in biomedical applications of titanium dioxide. *Phys. Chem. Chem. Phys.* **2013**, *15*, 4844−4858.

(3) Skocaj, M.; Filipic, M.; Petkovic, J.; Novak, S. Titanium dioxide in our everyday life; Is it safe? *Radiol. Oncol.* **2011**, *45*, 227−247.

(4) Baranowska-Wójcik, E.; Szwajgier, D.; Oleszczuk, P.; Winiarska-Mieczan, A. Effects of Titanium Dioxide Nanoparticles Exposure on Human Health—a Review. *Biol. Trace Elem. Res.* **2020**, *193*, 118−129.

(5) Koivisto, A. J.; et al. Industrial worker exposure to airborne particles during the packing of pigment and nanoscale titanium dioxide. *Inhalation Toxicol.* **2012**, *24*, 839−849.

(6) Guseva Canu, I.; Fraize-Frontier, S.; Michel, C.; Charles, S. Weight of epidemiological evidence for titanium dioxide risk assessment: current state and further needs. *J. Exposure Sci. Environ. Epidemiol.* **2020**, *30*, 430−435.

(7) Sahare, P.; et al. Engineered titania nanomaterials in advanced clinical applications. *Beilstein J. Nanotechnol.* **2022**, *13*, 201−218.

(8) Hou, J.; et al. Toxicity and mechanisms of action of titanium dioxide nanoparticles in living organisms. *J. Environ. Sci.* **2019**, *75*, 40.

(9) Iavicoli, I.; Leso, V.; Bergamaschi, A. Toxicological effects of titanium dioxide nanoparticles: A review of in vivo studies. *J. Nanomater.* **2012**, *2012*, 1.

(10) Husain, M.; et al. Intratracheally instilled titanium dioxide nanoparticles translocate to heart and liver and activate complement cascade in the heart of C57BL/6 mice. *Nanotoxicology* **2015**, *9*, 1013−1022.

(11) Chen, Z.; et al. Effect of titanium dioxide nanoparticles on the cardiovascular system after oral administration. *Toxicol. Lett.* **2015**, *239*, 123−130.

(12) Savi, M.; et al. Titanium dioxide nanoparticles promote arrhythmias via a direct interaction with rat cardiac tissue. *Part. Fibre Toxicol.* **2014**, *11*, 1.

(13) Rossi, S.; et al. Subchronic exposure to titanium dioxide nanoparticles modifies cardiac structure and performance in spontaneously hypertensive rats. *Part. Fibre Toxicol.* **2019**, *16*, 1.

(14) Xie, G.; Lu, W.; Lu, D. Penetration of titanium dioxide nanoparticles through slightly damaged skin in vitro and in vivo. *J. Appl. Biomater. Funct. Mater.* **2015**, *13*, e356−e361.

(15) Pelclova, D.; et al. NanoTiO2 sunscreen does not prevent systemic oxidative stress caused by UV radiation and a minor amount of NanoTiO2 is absorbed in humans. *Nanomaterials* **2019**, *9*, 888.

(16) Al-doaiss, A.; Jarrar, B.; Shati, A.; Al-kahtani, M.; Alfaifi, M. Cardiac and testicular alterations induced by acute exposure to titanium dioxide nanoparticles: Histopathological study. *IET Nanobiotechnol.* **2021**, *15*, 58−67.

(17) Liu, H.; et al. Biochemical toxicity of nano-anatase TiO_2 particles in mice. *Biol. Trace Elem. Res.* **2009**, *129*, 170−180.

(18) Weir, A.; Westerhoff, P.; Fabricius, L.; Hristovski, K.; Von Goetz, N. Titanium dioxide nanoparticles in food and personal care products. *Environ. Sci. Technol.* **2012**, *46*, 2242−2250.

(19) Cao, X.; et al. Foodborne Titanium Dioxide Nanoparticles Induce Stronger Adverse Effects in Obese Mice than Non-Obese

Mice: Gut Microbiota Dysbiosis, Colonic Inflammation, and Proteome Alterations. *Small* **2020**, *16*, 2001858.

(20) Crosera, M.; et al. Titanium dioxide nanoparticle penetration into the skin and effects on HaCaT cells. *Int. J. Environ. Res. Public Health* **2015**, *12*, 9282−9297.

(21) Colin-Val, Z.; et al. Titanium Dioxide (E171) Induces Toxicity in H9c2 Rat Cardiomyoblasts and Ex Vivo Rat Hearts. *Cardiovasc. Toxicol.* **2022**, *22*, 713−726.

(22) Katsumiti, A.; et al. Cytotoxicity of TiO₂ nanoparticles to mussel hemocytes and gill cells in vitro: Influence of synthesis method, crystalline structure, size and additive. *Nanotoxicology* **2015**, *9*, 543−553.

(23) Chellappa, M.; Anjaneyulu, U.; Manivasagam, G.; Vijayalakshmi, U. Preparation and evaluation of the cytotoxic nature of TiO₂ nanoparticles by direct contact method. *Int. J. Nanomed.* **2015**, *10*, 31−41.

(24) Huerta-García, E.; et al. Internalization of titanium dioxide nanoparticles is cytotoxic for H9c2 rat cardiomyoblasts. *Molecules* **2018**, *23*, 1955.

(25) Sayes, C. M.; et al. Correlating nanoscale titania structure with toxicity: A cytotoxicity and inflammatory response study with human dermal fibroblasts and human lung epithelial cells. *Toxicol. Sci.* **2006**, *92*, 174−185.

(26) Hattori, K.; et al. Exposure to nano-size titanium dioxide causes oxidative damages in human mesothelial cells: The crystal form rather than size of particle contributes to cytotoxicity. *Biochem. Biophys. Res. Commun.* **2017**, *492*, 218−223.

(27) Xiong, S.; et al. Specific surface area of titanium dioxide (TiO₂) particles influences cyto- and photo-toxicity. *Toxicology* **2013**, *304*, 132−140.

(28) Braydich-Stolle, L. K.; et al. Crystal structure mediates mode of cell death in TiO₂ nanotoxicity. *J. Nanopart. Res.* **2009**, *11*, 1361−1374.

(29) Wittmaack, K. In search of the most relevant parameter for quantifying lung inflammatory response to nanoparticle exposure: Particle number, surface area, or what? *Environ. Health Perspect.* **2007**, *115*, 187−194.

(30) Zhou, Y.; Hong, F.; Wang, L. Titanium dioxide nanoparticle-induced cytotoxicity and the underlying mechanism in mouse myocardial cells. *J. Nanopart. Res.* **2017**, *19*, 1−3.

(31) Hsiao, I.-L.; Huang, Y.-J. Effects of various physicochemical characteristics on the toxicities of ZnO and TiO₂ nanoparticles toward human lung epithelial cells. *Sci. Total Environ.* **2011**, *409*, 1219−1228.

(32) Zhao, H.; et al. Titanium dioxide nanoparticles induce mitochondrial dynamic imbalance and damage in HT22 cells. *J. Nanomater.* **2019**, *2019*, 1.

(33) Skubalova, Z.; et al. Prevalent anatase crystalline phase increases the cytotoxicity of biphasic titanium dioxide nanoparticles in mammalian cells. *Colloids Surf., B* **2019**, *182*, No. 110391.

(34) Watkins, S. J.; Borthwick, G. M.; Arthur, H. M. The H9C2 cell line and primary neonatal cardiomyocyte cells show similar hypertrophic responses in vitro. *Vitr. Cell. Dev. Biol. - Anim.* **2011**, *47*, 125−131.

(35) Kose, O.; et al. Impact of the Physicochemical Features of TiO₂ Nanoparticles on Their in Vitro Toxicity. *Chem. Res. Toxicol.* **2020**, *33*, 2324−2337.

(36) Yu, Q.; et al. Different toxicity of anatase and rutile TiO₂ nanoparticles on macrophages: Involvement of difference in affinity to proteins and phospholipids. *J. Hazard. Mater.* **2017**, *335*, 125−134.

(37) Zhang, H.; Banfield, J. F. Phase transformation of nanocrystalline anatase-to-rutile via combined interface and surface nucleation. *J. Mater. Res.* **2000**, *15*, 437−448.

(38) Murrieta, A. C.; Cavazos-Cavazos, D.; Santos-Aguilar, P.; Cholula-Díaz, J. L.; Contreras-Torres, F. F. Microstructure of polycrystalline gold nanoparticles and thin-films from a comparative X-ray line profile analysis. *Mater. Chem. Phys.* **2021**, *258*, No. 123976.

(39) Gubicza, J. *X-ray line profile analysis in Materials Science.* (IGI Global, 2014).

(40) Santos-Aguilar, P.; Contreras-Torres, F. F. X-ray diffraction line profile analysis: A microstructural study in polymorphic TiO₂. *Mater. Today: Proc.* **2019**, *13*, 420−427.

(41) Meißner, T.; Oelschlägel, K.; Potthoff, A. Dispersion of nanomaterials used in toxicological studies: A comparison of sonication approaches demonstrated on TiO₂ P25. *J. Nanopart. Res.* **2014**, *16*, 1−13.

(42) Wilkinson, M. D.; et al. Comment: The FAIR Guiding Principles for scientific data management and stewardship. *Sci. Data* **2016**, *3*, 1−9.

(43) Chhor, K.; Bocquet, J. F.; Pommier, C. Syntheses of submicron TiO₂ powders in vapor, liquid and supercritical phases, a comparative study. *Mater. Chem. Phys.* **1992**, *32*, 249−254.

(44) Wang, N.; Hsu, C.; Zhu, L.; Tseng, S.; Hsu, J.-P. Influence of metal oxide nanoparticles concentration on their zeta potential. *J. Colloid Interface Sci.* **2013**, *407*, 22−28.

(45) Zhang, Y.; Harris, C. X.; Wallenmeyer, P.; Murowchick, J.; Chen, X. Asymmetric lattice vibrational characteristics of rutile TiO₂ as revealed by laser power dependent raman spectroscopy. *J. Phys. Chem. C* **2013**, *117*, 24015−24022.

(46) Tian, F.; Zhang, Y.; Zhang, J.; Pan, C. Raman spectroscopy: A new approach to measure the percentage of anatase TiO₂ exposed (001) facets. *J. Phys. Chem. C* **2012**, *116*, 7515−7519.

(47) Bourikas, K.; Kordulis, C.; Lycourghiotis, A. Titanium dioxide (Anatase and Rutile): Surface chemistry, liquid-solid interface chemistry, and scientific synthesis of supported catalysts. *Chem. Rev.* **2014**, *114*, 9754−9823.

(48) Playford, H. Y. Variations in the local structure of nano-sized anatase TiO₂. *J. Solid State Chem.* **2020**, *288*, No. 121414.

(49) Kite, S. V.; et al. Nanostructured TiO₂ Sensitized with MoS₂ Nanoflowers for Enhanced Photodegradation Efficiency toward Methyl Orange. *ACS Omega* **2021**, *6*, 17071−17085.

(50) Igenepo John, K.; et al. Unravelling the effect of crystal dislocation density and microstrain of titanium dioxide nanoparticles on tetracycline removal performance. *Chem. Phys. Lett.* **2021**, *776*, No. 138725.

(51) O'Brien, J.; Wilson, I.; Orton, T.; Pognan, F. Investigation of the Alamar Blue (resazurin) fluorescent dye for the assessment of mammalian cell cytotoxicity. *Eur. J. Biochem.* **2000**, *267*, 5421−5426.

(52) Dikalov, S. I.; Harrison, D. G. Methods for detection of mitochondrial and cellular reactive oxygen species. *Antioxid. Redox Signaling* **2014**, *20*, 372−382.

(53) Jiang, J.; et al. Does nanoparticle activity depend upon size and crystal phase? *Nanotoxicology* **2008**, *2*, 33−42.

(54) Mukhopadhyay, P.; et al. Simultaneous detection of apoptosis and mitochondrial superoxide production in live cells by flow cytometry and confocal microscopy. *Nat. Protoc.* **2007**, *2*, 2295−2301.

(55) Miller, M. R.; Shaw, C. A.; Langrish, J. P. From particles to patients: Oxidative stress and the cardiovascular effects of air pollution. *Future Cardiol.* **2012**, *8*, 577−602.

(56) Yu, X.; Hong, F.; Zhang, Y.-Q. Bio-effect of nanoparticles in the cardiovascular system. *J. Biomed. Mater. Res., Part A* **2016**, *104*, 2881−2897.

(57) Wu, B.; Guo, C.; Zheng, N.; Xie, Z.; Stucky, G. D. Nonaqueous production of nanostructured anatase with high-energy facets. *J. Am. Chem. Soc.* **2008**, *130*, 17563−17567.

(58) Calatayud, M.; Minot, C. Effect of relaxation on structure and reactivity of anatase (100) and (001) surfaces. *Surf. Sci.* **2004**, *552*, 169−179.

(59) Lozano, O.; et al. Amorphous SiO₂ nanoparticles promote cardiac dysfunction via the opening of the mitochondrial permeability transition pore in rat heart and human cardiomyocytes. *Part. Fibre Toxicol.* **2020**, *17*, 1.

(60) Contreras-Torres, F. F.; et al. Differential cytotoxicity and internalization of graphene family nanomaterials in myocardial cells. *Mater. Sci. Eng. C* **2017**, *73*, 633−642.